The Tayler Instability in the Anelastic Approximation

J. Goldstein[1,2], R. H. D. Townsend[1,2], and E. G. Zweibel[1,3]

[1] Department of Astronomy, University of Wisconsin-Madison, 2535 Sterling Hall, 475 N. Charter Street, Madison, WI 53706, USA; jgoldstein@astro.wisc.edu
[2] Kavli Institute for Theoretical Physics, University of California, Santa Barbara, CA 93106, USA
[3] Department of Physics, University of Wisconsin-Madison, 2535 Chamberlin Hall, 1150 University Avenue, Madison, WI 53706, USA

Abstract

The Tayler instability (TI) is a non-axisymmetric linear instability of an axisymmetric toroidal magnetic field in magnetohydrostatic equilibrium (MHSE). In a differentially rotating radiative region of a star, the TI could drive the Tayler–Spruit dynamo, which generates magnetic fields that can significantly impact stellar structure and evolution. Heuristic prescriptions disagree on the efficacy of the dynamo, and numerical simulations have yet to definitively agree upon its existence. The criteria for the TI to develop were derived using fully compressible magnetohydrodynamics, while numerical simulations of dynamical processes in stars frequently use an anelastic approximation. This motivates us to derive new anelastic Tayler instability criteria. We find that some MHSE configurations are unstable in the fully compressible case but become stable in the anelastic case. We find and characterize the unstable modes of a simple family of cylindrical MHSE configurations using numerical calculations, and we discuss the implications for fully nonlinear anelastic simulations.

Key words: dynamo – instabilities – magnetic fields – magnetohydrodynamics (MHD) – stars: interiors – stars: magnetic field

1. Introduction

The Tayler instability (TI; Markey & Tayler 1973, 1974; Tayler 1973; Acheson 1978; Pitts & Tayler 1985) is a local non-axisymmetric linear instability of an axisymmetric toroidal magnetic field in magnetohydrostatic equilibrium (MHSE). Spruit (1999) has argued that this instability is particularly important because it can manifest when other instabilities are suppressed by thermal stratification. Growth rates are on the order of the global Alfvén-wave crossing time, which is generally short compared to other stellar timescales, even for weak magnetic fields. These two qualities make the TI the most relevant magnetic instability of a toroidal magnetic field in MHSE, at least in a non-rotating star.

The TI has been proposed as a mechanism for significantly affecting a stars' structure and rotational evolution. Aurière et al. (2007) proposed the TI as a mechanism to explain the observed dichotomy in the surface magnetic field strengths of intermediate-mass stars. In stars with a relatively weak poloidal field, differential rotation generates a toroidal field unstable to the TI, transforming the field components from low-order to high-order, and yielding disk-average surface fields that may fall below observational detection thresholds. Conversely, in stars with a relatively strong poloidal field, differential rotation decays before generating a toroidal field unstable to the TI, preserving the field components, and yielding low order surface fields seen in Ap/Bp stars.

Spruit (2002) proposed the TI as one half of a dynamo that could be a significant mechanism of angular momentum transport inside the radiative regions of stars. A toroidal field unstable to the TI generates a radial field displacement which is then rewound by differential rotation back into a toroidal field, creating a dynamo loop. The magnetic torque generated by this Tayler–Spruit dynamo could be a missing link in stellar evolution theory, where there is currently a discrepancy between the modeled and observed rotation rates of red giant cores, and of stellar remnants.

Cantiello et al. (2014) showed that the heuristic prescription for the Tayler–Spruit dynamo implemented in the stellar evolution code Modules for Experiments in Stellar Astrophysics (MESA; Paxton et al. 2013, 2015, 2018) increases angular momentum transport during red giant branch evolution. Although these results cannot fully explain the slow core rotation rates of red giant branch stars as observed by *Kepler*, the models with the dynamo are in better agreement with observations than the models without. Recently, Fuller et al. (2019) demonstrated that a revised prescription implemented into MESA could largely reproduce observed rotation rates.

Maeder & Meynet (2003, 2004, 2005) showed that a heuristic prescription for the Tayler–Spruit dynamo, as implemented in the Geneva stellar evolution code (Meynet & Maeder 2005), can have a significant effect on the main-sequence evolution of massive stars. The dynamo imposes near solid-body rotation that enhances meridional circulation and efficient mixing, resulting in larger convective cores, longer main-sequence life times, enriched surface abundances of nucleosynthesized elements, and elevated stellar luminosities. Song et al. (2016, 2018) demonstrated that for massive stars in binary systems, when spun up through tidal interactions, dynamo-induced solid-body rotation can lead to similar outcomes.

Despite the potential significance of the Tayler–Spruit dynamo in stellar structure and evolution, the existence and nature of the dynamo is currently debated through both analytical and numerical calculations. Analytically, various heuristic prescriptions have been developed to predict the magnitude of the magnetic torque (Spruit 1999, 2002; Maeder & Meynet 2003, 2004; Heger et al. 2005; Braithwaite 2006a; Denissenkov & Pinsonneault 2007). Numerically, nonlinear MHD simulations have been unable to agree whether the dynamo actually operates as envisaged (Braithwaite 2006b; Zahn et al. 2007).

In light of the potential importance of the Tayler–Spruit dynamo for stars, the disagreement between the analytical

predictions and the numerical results is unsettling. The discrepancy motivates us to look at the basic assumptions used in the original TI criteria and in the nonlinear MHD simulations investigating the Tayler–Spruit dynamo. Tayler (1973) developed criteria for the TI using fully compressible ideal MHD, while numerical MHD simulations of stellar interiors frequently use anelastic MHD (e.g., Brown et al. 2012). This approximation filters out sound waves, which are very short-period relative to stellar timescales and are therefore prohibitively expensive to compute.

The goal of this paper is to re-examine the TI in the anelastic approximation. We derive new anelastic TI (anTI) stability criteria and we then apply them to a family of simple MHSE models to determine which are subject to the instability. We verify our results numerically using a modified version of the GYRE stellar oscillation code (Townsend & Teitler 2013), which solves a system of linearized anelastic MHD equations to calculate growth rates and eigenfunctions of unstable modes. We conclude that the anelastic case is more restrictive but that the TI should be present in anelastic MHD simulations if the models used are unstable under the anTI criteria.

This paper is structured as follows. In Section 2, we give an overview of the energy principle, which is the method that, following Tayler (1973), we have used to develop the instability criteria. In Section 3, we introduce the fully compressible MHD equations and the Lantz–Braginsky–Roberts (LBR) anelastic approximation for MHD, which is a form that is valid in the isothermal atmosphere that we assume in our later analysis. In Section 4, we summarize the original TI stability criteria derived from the energy principle and we derive the new anTI criteria. In Section 5, we compare the original and anTI criteria to GYRE's numerically calculated growth rates and eigenfunctions for unstable modes in our models, showing that the anTI criteria are correct in anelastic MHD. In Section 6, we conclude with considerations for future analytical and numerical work.

2. Energy Principle

The instability analysis in Tayler (1973) was developed using the MHD energy principle of Bernstein et al. (1958), which gives the necessary and sufficient condition for an energy-conserving, ideal system in MHSE to be unstable to small displacements. Although the energy principle is widely used in studies of laboratory and natural plasmas, we will need to modify it to accommodate the anelastic equations, so we will briefly review it here.

The energy principle is based on being able to write the linearized equation of motion for the fluid displacement perturbation, $\boldsymbol{\xi}$, in the form

$$\rho \frac{\partial^2 \boldsymbol{\xi}}{\partial t^2} = \boldsymbol{F}(\boldsymbol{\xi}), \qquad (1)$$

where $\boldsymbol{\xi}$ is related to velocity perturbations $\boldsymbol{u}'$ by

$$\boldsymbol{u}' = \frac{\partial \boldsymbol{\xi}}{\partial t}, \qquad (2)$$

and $\boldsymbol{F}$ is a linear, self-adjoint operator.[4] Since Equation (1) does not explicitly depend on time, we look for separable

---
[4] By self adjointness we mean $\int \boldsymbol{\xi} \cdot \boldsymbol{F}(\boldsymbol{\eta}) \, d\tau = \int \boldsymbol{\eta} \cdot \boldsymbol{F}(\boldsymbol{\xi}) \, d\tau$ for displacement vectors $\boldsymbol{\xi}, \boldsymbol{\eta}$ that obey suitable boundary conditions.

solutions of the form

$$\boldsymbol{\xi}(t) \propto \exp i\omega t, \qquad (3)$$

where ω is an angular frequency. It follows from the self adjointness property that ω^2 is real; $\omega^2 < 0$ signifies instability, with an exponential growth rate $\lambda = |\omega|$.

It can be shown that Equation (1), together with the self adjointness property, leads to a conservation law which we identify with conservation of perturbation energy:

$$\frac{\partial}{\partial t} \left[\frac{1}{2} \int \rho \frac{\partial \boldsymbol{\xi}}{\partial t} \cdot \frac{\partial \boldsymbol{\xi}}{\partial t} \, d\tau - \frac{1}{2} \int \boldsymbol{\xi} \cdot \boldsymbol{F}(\boldsymbol{\xi}) \, d\tau \right] = 0. \qquad (4)$$

The first term in brackets in Equation (4) is the kinetic energy δK, while the second represents the potential energy

$$\delta W = -\frac{1}{2} \int \boldsymbol{\xi} \cdot \boldsymbol{F}(\boldsymbol{\xi}) \, d\tau. \qquad (5)$$

Equation (4) shows that $\delta K + \delta W$ is constant in time. For an unstable mode, both δK and δW grow exponentially in magnitude with time, and δK is positive definite; therefore, δW must be negative. This is the basis of the energy principle.

The energy principle has both advantages and disadvantages when compared to solving for the eigenvalues ω^2 of Equation (1). The advantage is that it is often easier to minimize δW, or even evaluate it for a set of trial functions, than to solve the coupled set of differential equations corresponding to the eigenvalue problem and hope to capture all modes. The disadvantage is that the energy principle yields at best the lowest-eigenvalue mode (obtained by rigorous minimization of δW) rather than the whole spectrum of stable and unstable modes.

3. Fully Compressible and Anelastic Ideal MHD

Fully compressible, isentropic, ideal MHD is described by the conservation equations for mass, momentum, and entropy, together with Faraday–Maxwell's Law (combined with Ohm's Law), Ampère's Law, and Gauss" Law for magnetism,

$$\frac{\partial \rho}{\partial t} + \nabla \cdot (\rho \boldsymbol{u}) = 0, \qquad (6)$$

$$\frac{\partial \boldsymbol{u}}{\partial t} + \boldsymbol{u} \cdot \nabla \boldsymbol{u} = -\frac{1}{\rho} \nabla P + \boldsymbol{g} + \frac{\boldsymbol{J} \times \boldsymbol{B}}{\rho c}, \qquad (7)$$

$$\frac{\partial S}{\partial t} + \boldsymbol{u} \cdot \nabla S = 0, \qquad (8)$$

$$\frac{\partial \boldsymbol{B}}{\partial t} = \nabla \times (\boldsymbol{u} \times \boldsymbol{B}), \qquad (9)$$

$$\boldsymbol{J} = \frac{c}{4\pi} \nabla \times \boldsymbol{B}, \qquad (10)$$

$$\nabla \cdot \boldsymbol{B} = 0. \qquad (11)$$

Here, $\boldsymbol{u}$, ρ, P, S, $\boldsymbol{g}$, $\boldsymbol{B}$ and $\boldsymbol{J}$ are the fluid velocity, density, pressure, specific entropy, gravitational acceleration, magnetic field and current density, respectively. The pressure, density and specific entropy are assumed to be related by the equation of state

$$\rho = \rho(S, P), \qquad (12)$$

which for simplicity we assume to follow ideal-gas behavior.

To model the evolution of small perturbations of a static equilibrium state, we decompose the dependent variables into

the sum of a background value (denoted by the subscript 0), and a perturbed value (denoted by a prime):

$$
\begin{aligned}
\boldsymbol{u} &= \boldsymbol{u}', \\
P &= P_0 + P', \\
\rho &= \rho_0 + \rho', \\
S &= S_0 + S', \\
\boldsymbol{B} &= \boldsymbol{B}_0 + \boldsymbol{B}', \\
\boldsymbol{J} &= \boldsymbol{J}_0 + \boldsymbol{J}'
\end{aligned}
\tag{13}
$$

(we neglect any perturbations to the gravity $\boldsymbol{g}$). The background values obey the MHSE condition

$$
\frac{\nabla P_0}{\rho_0} = \boldsymbol{g} + \frac{\boldsymbol{J}_0 \times \boldsymbol{B}_0}{\rho_0 c}, \tag{14}
$$

the equilibrium current equation

$$
\boldsymbol{J}_0 = \frac{c}{4\pi} \nabla \times \boldsymbol{B}_0, \tag{15}
$$

and a gradient relation that follows from the equation of state (12),

$$
\frac{\nabla \rho_0}{\rho_0} = \frac{\nabla P_0}{\gamma P_0} - \frac{\nabla S_0}{c_P}, \tag{16}
$$

where c_P is the specific heat at constant pressure and γ is the ratio of specific heats. Likewise, the perturbed values satisfy the linearized ideal MHD equations that follow when we substitute the expressions (13) into Equations (6)–(11)), subtract the background state, and discard terms that are second- or higher-order in perturbed quantities:

$$
\frac{\partial \rho'}{\partial t} + \nabla \cdot (\rho_0 \boldsymbol{u}') = 0, \tag{17}
$$

$$
\frac{\partial \boldsymbol{u}'}{\partial t} = -\frac{\nabla P'}{\rho_0} + \frac{\rho'}{\rho_0}\boldsymbol{g} + \left(\frac{\boldsymbol{J}' \times \boldsymbol{B}_0 + \boldsymbol{J}_0 \times \boldsymbol{B}'}{\rho_0 c} \right), \tag{18}
$$

$$
\frac{\partial S'}{\partial t} + \boldsymbol{u}' \cdot \nabla S_0 = 0, \tag{19}
$$

$$
\frac{\partial \boldsymbol{B}'}{\partial t} = \nabla \times (\boldsymbol{u}' \times \boldsymbol{B}_0), \tag{20}
$$

$$
\boldsymbol{J}' = \frac{c}{4\pi} (\nabla \times \boldsymbol{B}'), \tag{21}
$$

$$
\nabla \cdot \boldsymbol{B}' = 0. \tag{22}
$$

Numerical MHD simulations that are relevant on stellar scales of interest frequently use an anelastic approximation,

$$
\nabla \cdot (\rho_0 \boldsymbol{u}') = 0, \tag{23}
$$

that filters out fast, high-frequency sound waves unimportant on stellar scales, while keeping slower internal gravity waves. The anelastic approximation is technically valid only for adiabatically stratified systems ($\nabla S_0 = 0$), but is now used to study problems such as penetrative convection and interface dynamos that include stably stratified regions. In such contexts, Brown et al. (2012) studied energy conservation in three widely used forms of the anelastic equations. They showed that one, the so-called LBR formulation (Lantz 1992; Braginsky & Roberts 1995) conserves energy, while the others conserve a related but distinct pseudo-energy. Therefore, we consider the LBR formulation to be the best candidate for analyzing the

Taylor instability in the anelastic approximation, and study only that version in this paper. However, as we will see, the energy principle has to be modified, even for the LBR formulation.

The LBR formulation re-writes the linearized momentum equation in terms of entropy and a reduced pressure perturbation

$$
\varpi' \equiv \frac{P'}{\rho_0}, \tag{24}
$$

and neglects a term $\varpi' \nabla(S_0/c_P)$. Although Brown et al. (2012) neglected the effect of magnetic fields, it can be shown by recapitulating their analysis that neglecting *all* terms proportional to ϖ' (but not its gradient) in the linearized momentum equation preserves energy conservation in an isothermal atmosphere, even in the presence of magnetic fields.

We develop an LBR version of the linearized momentum Equation (18) by eliminating the density perturbation using the linearized equation of state,

$$
\frac{\rho'}{\rho_0} = \frac{1}{\gamma}\frac{P'}{P_0} - \frac{S'}{c_P}, \tag{25}
$$

and likewise eliminating the background pressure gradient ∇P_0 using the MHSE condition (14). The linearized momentum equation then becomes

$$
\frac{\partial \boldsymbol{u}'}{\partial t} = -\nabla \varpi' - \frac{S'}{c_P}\boldsymbol{g} + \left(\frac{\boldsymbol{J}' \times \boldsymbol{B}_0 + \boldsymbol{J}_0 \times \boldsymbol{B}'}{\rho_0 c} \right), \tag{26}
$$

where, as discussed above, we have dropped all terms proportional to ϖ'. The linearized LBR anelastic MHD equations then comprise Equations (19)–(23) and (26).

4. Instability Analysis

4.1. Fully Compressible Analysis

Tayler (1973) derived his criteria for stability by applying a fully compressible MHD form of the energy principle (see Section 2) to an equilibrium configuration comprising an axisymmetric toroidal magnetic field in a non-rotating stratified plasma. In this configuration, all background quantities are functions only of the cylindrical radial (r) and axial (z) coordinates. Here, we briefly recapitulate his analysis. First, we integrate Equations (17) and (20) with respect to time to obtain explicit expressions for the density, magnetic field and current perturbations in terms of the displacement vector $\boldsymbol{\xi}$,

$$
\rho' = -\nabla \cdot (\rho_0 \boldsymbol{\xi}), \tag{27}
$$

$$
\boldsymbol{B}' = \nabla \times (\boldsymbol{\xi} \times \boldsymbol{B}_0), \tag{28}
$$

$$
\boldsymbol{J}' = \frac{c}{4\pi} \nabla \times [\nabla \times (\boldsymbol{\xi} \times \boldsymbol{B}_0)]. \tag{29}
$$

The linearized equation of state (25) leads to a corresponding expression for the pressure perturbation,

$$
P' = -\gamma P_0 \nabla \cdot \boldsymbol{\xi} - \boldsymbol{\xi} \cdot \nabla P_0. \tag{30}
$$

By substituting these expressions into the linearized momentum Equation (18), the force operator introduced in

Equation (1) is found as

$$\boldsymbol{F}(\boldsymbol{\xi}) = \nabla(\gamma P_0 \nabla \cdot \boldsymbol{\xi} + \boldsymbol{\xi} \cdot \nabla P_0) - \nabla \cdot (\rho_0 \boldsymbol{\xi})\, \boldsymbol{g}$$
$$+ \frac{1}{4\pi}[(\nabla \times \boldsymbol{B}') \times \boldsymbol{B}_0 + (\nabla \times \boldsymbol{B}_0) \times \boldsymbol{B}']. \quad (31)$$

Kulsrud (1964) demonstrated that this force operator is self-adjoint under boundary conditions

$$\boldsymbol{\xi} \cdot \hat{\boldsymbol{n}} = 0, \qquad \boldsymbol{B}_0 \cdot \hat{\boldsymbol{n}} = 0, \quad (32)$$

that correspond to rigid, perfectly conducting walls; here, $\hat{\boldsymbol{n}}$ is the unit surface normal vector of the boundary.

Taking the scalar product of Equation (31) with $\boldsymbol{\xi}$, and integrating over volume, leads via Equation (5) to the potential energy

$$\delta W = \frac{1}{2} \int d\tau \left[\frac{\boldsymbol{B}'^2}{4\pi} - \frac{\boldsymbol{J}_0 \cdot (\boldsymbol{B}' \times \boldsymbol{\xi})}{c} + \gamma P_0 (\nabla \cdot \boldsymbol{\xi})^2 \right.$$
$$\left. + (\boldsymbol{\xi} \cdot \nabla P_0)\, \nabla \cdot \boldsymbol{\xi} + (\boldsymbol{\xi} \cdot \boldsymbol{g})\, \nabla \cdot (\rho_0 \boldsymbol{\xi}) \right], \quad (33)$$

where we have made use of the boundary conditions (32) to eliminate surface integrals involving $\boldsymbol{\xi} \cdot \hat{\boldsymbol{n}}$ and $\boldsymbol{B}_0 \cdot \hat{\boldsymbol{n}}$.

Following Tayler (1973), we write the fluid displacement vector in cylindrical coordinates as

$$\begin{bmatrix} \xi_r \\ \xi_\phi \\ \xi_z \end{bmatrix} = \begin{bmatrix} X \cos m\phi \\ -(Y/m)\sin m\phi \\ Z \cos m\phi \end{bmatrix}, \quad (34)$$

where X, Y, Z are real functions of r and z, and the integer m is an azimuthal wavenumber. With these definitions, we evaluate the ϕ part of the integral in Equation (33) to obtain

$$\delta W = \frac{1}{8} \int r\, dr\, dz \left\{ \frac{m^2 B_\phi^2}{r^2}(X^2 + Z^2) \right.$$
$$+ \left[\frac{\partial}{\partial r}(B_\phi X) + \frac{\partial}{\partial z}(B_\phi Z) \right]^2$$
$$- \left[\frac{\partial}{\partial r}(B_\phi X) + \frac{\partial}{\partial z}(B_\phi Z) \right]\left[\frac{1}{r}\frac{\partial}{\partial r}(rB_\phi)X + \frac{\partial B_\phi}{\partial z}Z \right]$$
$$- \frac{B_\phi}{r}Y\left[\frac{1}{r}\frac{\partial}{\partial r}(rB_\phi)X + \frac{\partial B_\phi}{\partial z}Z \right]$$
$$+ 4\pi\gamma P_0 \left[\frac{1}{r}\frac{\partial}{\partial r}(rX) - \frac{Y}{r} + \frac{\partial Z}{\partial z} \right]^2$$
$$+ 4\pi(g_r X + g_z Z)\left(\frac{\partial \rho_0}{\partial r}X + \frac{\partial \rho_0}{\partial z}Z \right)$$
$$+ 4\pi\left[X\left(\frac{\partial P_0}{\partial r} + \rho_0 g_r \right) + Z\left(\frac{\partial P_0}{\partial z} + \rho_0 g_z \right) \right]$$
$$\left. \times \left[\frac{1}{r}\frac{\partial}{\partial r}(rX) - \frac{Y}{r} + \frac{\partial Z}{\partial z} \right] \right\}, \quad (35)$$

where g_r and g_z are the radial and axial components of the background gravity $\boldsymbol{g}$, respectively, and B_ϕ is the azimuthal component of the background field $\boldsymbol{B}_0$. This expression is minimized with respect to Y by solving

$$\frac{\partial \delta W}{\partial Y} = 0, \quad (36)$$

to obtain

$$\frac{Y}{r} = \frac{1}{r}\frac{\partial}{\partial r}(rX) + \frac{\partial Z}{\partial z} + \frac{\rho_0}{\gamma P_0}(g_r X + g_z Z). \quad (37)$$

By substituting this back into Equation (35), the minimized potential energy is found as

$$\delta W_{\mathrm{min}} = \frac{1}{8} \int r\, dr\, dz \left\{ B_\phi^2 \left[r\frac{d}{dr}\left(\frac{X}{r} \right) + \frac{dZ}{dz} \right]^2 \right.$$
$$\left. + 4\pi[\mathcal{A}X^2 + \mathcal{B}XZ + \mathcal{C}Z^2] \right\} \quad (38)$$

where we introduce

$$\mathcal{A} \equiv -\rho_0 g_r\left(\frac{\rho_0 g_r}{\gamma P_0} - \frac{1}{\rho_0}\frac{\partial \rho_0}{\partial r} \right)$$
$$+ m^2 \frac{B_\phi^2}{4\pi r^2} - \frac{B_\phi}{2\pi r^2}\frac{\partial}{\partial r}(rB_\phi),$$
$$\mathcal{B} \equiv -\rho_0 g_r\left(\frac{\rho_0 g_z}{\gamma P_0} - \frac{1}{\rho_0}\frac{\partial \rho_0}{\partial z} \right)$$
$$- \rho_0 g_z\left(\frac{\rho_0 g_r}{\gamma P_0} - \frac{1}{\rho_0}\frac{\partial \rho_0}{\partial r} \right) - \frac{B_\phi}{2\pi r}\frac{\partial B_\phi}{\partial z},$$
$$\mathcal{C} \equiv -\rho_0 g_z\left(\frac{\rho_0 g_z}{\gamma P_0} - \frac{1}{\rho_0}\frac{\partial \rho_0}{\partial z} \right) + m^2 \frac{B_\phi^2}{4\pi r^2}. \quad (39)$$

The first term in the integrand of Equation (38) is positive definite. For the remaining terms, which appear as a quadratic form in X and Z, the sufficient conditions that $\delta W_{\mathrm{min}} > 0$ are that

$$\mathcal{A} > 0, \qquad \mathcal{C} > 0, \qquad 4\mathcal{A}\mathcal{C} > \mathcal{B}^2 \quad (40)$$

everywhere. These are the criteria for *stability* against the TI. Since the azimuthal order m appears only in the positive-definite terms $m^2 B_\phi^2 / 4\pi r^2$ in Equation (39), the most unstable non-axisymmetric modes correspond to $|m| = 1$. For these modes, the above expressions reduce to the criteria given by Tayler (1973, his Equations (2.20)–(2.22), modulo factors of 4π that arise from our choice of electromagnetic units. As Tayler demonstrates in his Appendix 2, the above criteria are not only sufficient but also necessary given that violation of one or more of these inequalities can lead to instability ($\delta W_{\mathrm{min}} < 0$) for a suitable choice of X and Z.

4.2. Constrained Analysis

We now consider how to implement the anelastic constraint in our analysis. This constraint removes the freedom to choose a Y that minimizes δW; instead, we must set

$$\frac{Y}{r} = \frac{1}{r}\frac{\partial}{\partial r}(rX) + \frac{\partial Z}{\partial z} + \frac{1}{\rho_0}\frac{d\rho_0}{dr}X + \frac{1}{\rho_0}\frac{d\rho_0}{dz}Z \quad (41)$$

to ensure that Equation (23) is satisfied. We repeat the analysis of the preceding section, but using this expression in place of Equation (37) yields a potential energy that is identical to

Equation (38), save that the quadratic-form coefficients $\mathcal{A}$, $\mathcal{B}$ and $\mathcal{C}$ are replaced by

$$\mathcal{A}_c \equiv \mathcal{A} + \gamma P_0 \left(\frac{\rho_0 g_r}{\gamma P_0} - \frac{1}{\rho_0} \frac{\partial \rho_0}{\partial r} \right)^2,$$

$$\mathcal{B}_c \equiv \mathcal{B} + 2\gamma P_0 \left(\frac{\rho_0 g_r}{\gamma P_0} - \frac{1}{\rho_0} \frac{\partial \rho_0}{\partial r} \right) \left(\frac{\rho_0 g_z}{\gamma P_0} - \frac{1}{\rho_0} \frac{\partial \rho_0}{\partial z} \right),$$

$$\mathcal{C}_c \equiv \mathcal{C} + \gamma P_0 \left(\frac{\rho_0 g_z}{\gamma P_0} - \frac{1}{\rho_0} \frac{\partial \rho_0}{\partial z} \right)^2, \tag{42}$$

respectively (here, the "c" subscripts stand for "constrained"). The criteria for stability are now that

$$\mathcal{A}_c > 0, \qquad \mathcal{C}_c > 0, \qquad 4\mathcal{A}_c \mathcal{C}_c > \mathcal{B}_c^2. \tag{43}$$

As we will demonstrate in Section 5, these constrained TI (cTI) criteria under-predict the extent of the instability found by numerical calculations employing the anelastic condition. This shortcoming motivates a more careful treatment, based on re-deriving the force operator from the LBR anelastic linearized momentum Equation (26).

4.3. LBR Anelastic Analysis

To re-derive the force operator in the LBR anelastic case, first we integrate Equation (19) with respect to time to obtain

$$S' = -\boldsymbol{\xi} \cdot \nabla S_0. \tag{44}$$

By substituting this expression and Equations (27)–(30) into the linearized momentum Equation (26), the LBR anelastic force operator is derived as

$$\boldsymbol{F}_{\mathrm{LBR}}(\boldsymbol{\xi}) = -\rho_0 \nabla \varpi' - \rho_0 \boldsymbol{g}\, \boldsymbol{\xi} \cdot \left[\frac{\nabla P_0}{\gamma P_0} - \frac{\nabla \rho_0}{\rho_0} \right]$$
$$+ \frac{1}{4\pi} [(\nabla \times \boldsymbol{B}') \times \boldsymbol{B}_0 + (\nabla \times \boldsymbol{B}_0) \times \boldsymbol{B}'], \tag{45}$$

where we have used Equation (16) to eliminate the background entropy gradient ∇S_0. This operator is self-adjoint under the same boundary conditions (32) as applied before.

We repeat the analysis of Section 4.1, but using Equations (41), (45) in place of (31), (37). The resulting potential energy is identical to Equation (38), save that the quadratic-form coefficients $\mathcal{A}$, $\mathcal{B}$ and $\mathcal{C}$ are now replaced by

$$\mathcal{A}_{\mathrm{LBR}} \equiv \mathcal{A} + \frac{B_\phi}{4\pi r} \frac{\partial}{\partial r}(r B_\phi) \left(\frac{\rho_0 g_r}{\gamma P_0} - \frac{1}{\rho_0} \frac{\partial \rho_0}{\partial r} \right),$$

$$\mathcal{B}_{\mathrm{LBR}} \equiv \mathcal{B} + \frac{B_\phi}{4\pi} \frac{\partial B_\phi}{\partial z} \left(\frac{\rho_0 g_r}{\gamma P_0} - \frac{1}{\rho_0} \frac{\partial \rho_0}{\partial r} \right)$$
$$+ \frac{B_\phi}{4\pi r} \frac{\partial}{\partial r}(r B_\phi) \left(\frac{\rho_0 g_z}{\gamma P_0} - \frac{1}{\rho_0} \frac{\partial \rho_0}{\partial z} \right),$$

$$\mathcal{C}_{\mathrm{LBR}} \equiv \mathcal{C} + \frac{B_\phi}{4\pi} \frac{\partial B_\phi}{\partial z} \left(\frac{\rho_0 g_z}{\gamma P_0} - \frac{1}{\rho_0} \frac{\partial \rho_0}{\partial z} \right), \tag{46}$$

respectively. The criteria for stability against the TI are now that

$$\mathcal{A}_{\mathrm{LBR}} > 0, \qquad \mathcal{C}_{\mathrm{LBR}} > 0, \qquad 4\mathcal{A}_{\mathrm{LBR}} \mathcal{C}_{\mathrm{LBR}} > \mathcal{B}_{\mathrm{LBR}}^2. \tag{47}$$

Using the same approach as in Appendix 2 of Tayler (1973), we can show that these anelastic TI (anTI) criteria are necessary and also sufficient. We note that the most unstable non-axisymmetric modes still correspond to $|m| = 1$. Together, Equations (46) and (47) make up the principal result of this paper.

5. Numerical Instability Calculations

In this section, we compare the analytic work in the preceding sections against numerical solutions of the linearized LBR anelastic MHD equations and boundary conditions. Details of our numerical technique are given in the Appendix; in brief, we modify the GYRE stellar oscillation code (Townsend & Teitler 2013) to find the modal eigenvalues and eigenfunctions. Because the GYRE code is restricted to solving 1D eigenproblems, we focus our analysis on a reduced equilibrium case in which background quantities depend only on r.

5.1. Equilibrium Model

The 1D equilibrium model that we consider assumes an isothermal stratification characterized by a constant sound speed a and a constant ratio β of gas pressure to magnetic pressure. Radial gravity is provided by a line mass on the cylindrical axis of symmetry,

$$g_r(r) = -\frac{qa^2}{r} \tag{48}$$

where $q \geqslant 0$ is a dimensionless gravitational strength parameter. Solving the MHSE Equation (14) yields a power-law background pressure distribution

$$P_0(r) = P_{0,0} \left(\frac{r}{r_0} \right)^{-\alpha}, \tag{49}$$

where $P_{0,0}$ is the pressure at some fiducial radius r_0, and

$$\alpha \equiv \frac{2 + q\beta}{1 + \beta}. \tag{50}$$

The background density and azimuthal field strength are

$$\rho_0(r) = \frac{P_0(r)}{a^2} \tag{51}$$

and

$$B_\phi(r) = \left[\frac{8\pi P_0(r)}{\beta} \right]^{1/2}, \tag{52}$$

respectively.

It can be shown that for $\alpha < 2$, the magnetic tension in this equilibrium model dominates the magnetic pressure, meaning that the stratification is both magnetically and gravitationally confined. To satisfy $\alpha < 2$, from Equation (50), the gravitational parameter must be $q < 1$. For stars, of course, we expect that the magnetic field is relatively weak and that the equilibrium is close to hydrostatic, whether the magnetic field provides pressure support through its negative gradient or confinement through tension.

In the context of the 1D equilibrium model described here, the quadratic coefficients (39) for the stability criteria in the

fully compressible case become

$$\mathcal{A} = \left[q\left(\alpha - \frac{q}{\gamma} \right) + \frac{2}{\beta}(\alpha + m^2 - 2) \right] \frac{P_0}{r^2},$$

$$\mathcal{B} = 0, \qquad \mathcal{C} = \frac{2m^2}{\beta} \frac{P_0}{r^2}. \qquad (53)$$

The stability criteria (40) then reduce to the requirement that the bracketed term in the expression for $\mathcal{A}$ be positive.

For the constrained anelastic and LBR anelastic cases, the corresponding expressions are

$$\mathcal{A}_{\mathrm{c}} = \left[q\left(\alpha - \frac{q}{\gamma} \right) + \frac{2}{\beta}(\alpha + m^2 - 2) + \frac{(q - \alpha\gamma)^2}{\gamma} \right] \frac{P_0}{r^2},$$

$$\mathcal{B}_{\mathrm{c}} = 0, \qquad \mathcal{C}_{\mathrm{c}} = \frac{2m^2}{\beta} \frac{P_0}{r^2},$$

$$(54)$$

and

$$\mathcal{A}_{\mathrm{LBR}} = \left[q\left(\alpha - \frac{q}{\gamma} \right) + \frac{2}{\beta}(\alpha + m^2 - 2) \right.$$

$$\left. + \frac{(\alpha - 2)(q - \alpha\gamma)}{\beta\gamma} \right] \frac{P_0}{r^2},$$

$$\mathcal{B}_{\mathrm{LBR}} = 0, \qquad \mathcal{C}_{\mathrm{LBR}} = \frac{2m^2}{\beta} \frac{P_0}{r^2}, \qquad (55)$$

respectively. As before, the stability criteria reduce to the requirement that the bracketed terms are positive.

5.2. Stable and Unstable Modes

As an initial demonstration of our numerical solution technique, we calculate eigenvalues and eigenfunctions of stable and unstable modes for an equilibrium configuration having $\beta = 5$, $q = 0.01$ and $\gamma = 5/3$. This choice of parameters ensures that we are looking at a robust instability, as we shall later show in a parameter study. We solve the linearized equations and boundary conditions on a spatial grid of 1000 points, uniformly spanning the domain $[\tilde{r}_a, \tilde{r}_b] = [1, 1.5]$ (here, $\tilde{r}$ is the dimensionless radius introduced in the Appendix). Assuming an azimuthal wavenumber $m = 1$ and an axial wavenumber $k = 25$, we search for modes having eigenvalues $\tilde{\omega}^2$ below the square $\tilde{\omega}_A^2$ of the dimensionless Alfvén frequency evaluated at $\tilde{r} = \tilde{r}_b$ (see Equation (76)). These modes comprise an infinite family, in which each mode can be uniquely classified by a radial order n that counts the number of nodes (excluding the endpoints) in the dimensionless radial displacement eigenfunction $\tilde{\xi}_r$. With this classification, an ordering by n is in one-to-one correspondence with an ordering by $\tilde{\omega}^2$, with the eigenvalue $\tilde{\omega}_0^2$ of the $n = 0$ (fundamental) mode being the least positive.

Figure 1 plots the dimensionless displacement eigenfunctions, $\tilde{\xi}_r$, $\tilde{\xi}_\phi$, and $\tilde{\xi}_z$, as a function of $\tilde{r}$ for the three lowest-order modes ($n = 0, 1, 2$). Each plot is labeled at top-left by the corresponding eigenvalue $\tilde{\omega}_n^2$. From these eigenvalues, we see that the fundamental mode and first overtone ($n = 1$) are both unstable, with $\tilde{\omega}^2 < 0$. From the eigenfunctions, we see that the displacement in the azimuthal direction is greater than that in the radial direction, $|\tilde{\xi}_\phi| > |\tilde{\xi}_r|$, as predicted by Spruit (2002).
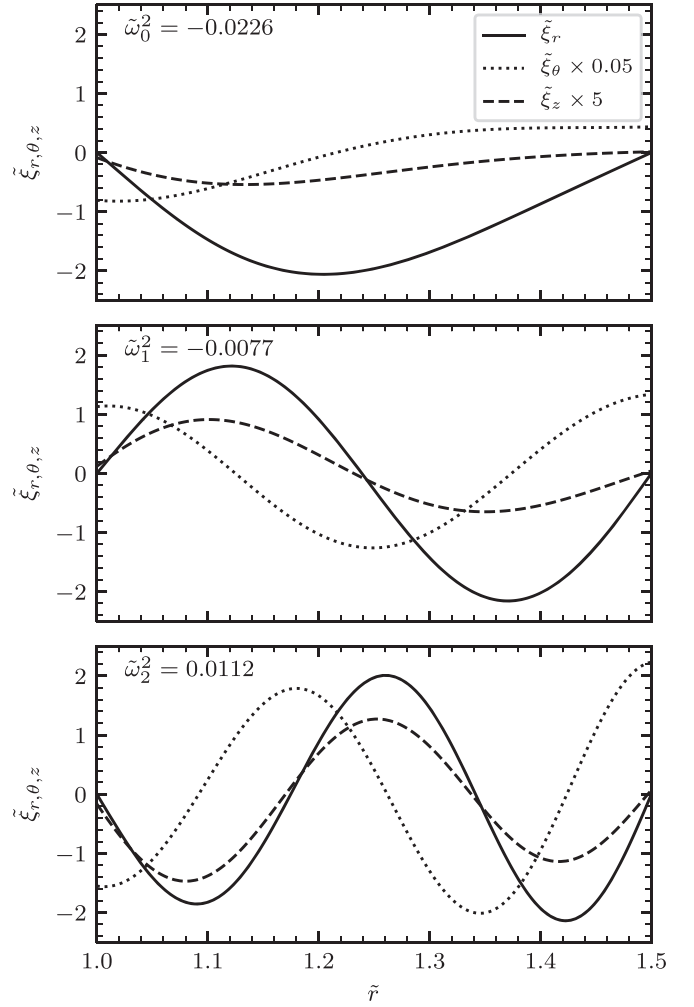

Figure 1. Dimensionless displacement eigenfunctions of the $n = 0, 1, 2$ modes (top to bottom), for an azimuthal wavenumber $m = 1$ and an axial wavenumber $k = 25$, and an equilibrium model having $\beta = 5$, $q = 0.01$ and $\gamma = 5/3$. In each panel, the eigenfunctions are normalized such that the root-mean-square value of $\tilde{\xi}_r$ is unity. The plots are labeled with the corresponding eigenvalue $\tilde{\omega}_n^2$; negative values for the $n = 0$ and $n = 1$ modes indicates that they are unstable.

This makes sense because displacement along the magnetic field lines on equipotential gravitational surfaces does not need to do work against the stratification.

5.3. Dependence on Axial Wavenumber

We now explore how the mode eigenvalues depend on the axial wavenumber k. With other parameters fixed at the values given in Section 5.2, Figure 2 plots the eigenvalues of unstable modes as a function of k. The plot shows that for modes with a given radial order n to become unstable, k must exceed some finite threshold k_n. Above this threshold, the eigenvalue decreases monotonically with k, approaching an asymptotic limit as $k \to \infty$. This is similar behavior to that found by Pitts & Tayler (1985) for a uniform-density incompressible fluid without gravity. In a non-ideal fluid with one or more forms of diffusion (thermal, viscous, or resistive), diffusive damping is expected to reduce the instability of modes at high k, leading to a minimal $\tilde{\omega}^2 < 0$ (i.e., maximal growth rate) at large but finite k.
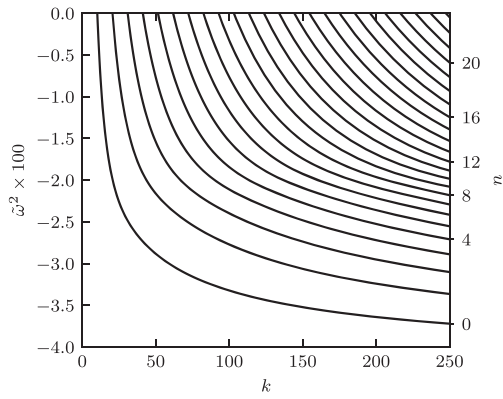
Figure 2. Eigenvalues $\tilde{\omega}^2$ plotted as a function of axial wavenumber k, for an azimuthal wavenumber $m = 1$ and an equilibrium model having $\beta = 5$, $q = 0.01$ and $\gamma = 5/3$. Selected modes are labeled at right with their radial order n.

5.4. Stability Boundaries

Because the fundamental mode is the most unstable at any k, we can use it as a proxy for the onset of the TI. Accordingly, we evaluate the minimal eigenvalue $\tilde{\omega}_{\min}^2$, over all modes, as the limiting value of the fundamental-mode eigenvalue in the limit $k \to \infty$:

$$\tilde{\omega}_{\min}^2 = \lim_{k \to \infty} \tilde{\omega}_0^2. \tag{56}$$

When $\tilde{\omega}_{\min}^2 < 0$, the maximal exponential growth rate of the Tayler instability is then given by

$$\lambda_{\max} = \frac{a|\tilde{\omega}_{\min}|}{r_0}. \tag{57}$$

Because our numerical calculations are restricted to finite values of k, we estimate the limit on the right-hand side of Equation (56) by evaluating $\tilde{\omega}_0^2$ at $k = 1000$ and $k = 2000$, and then linearly extrapolating in inverse wavenumber k^{-1} to find the eigenvalue at $k^{-1} \to 0$.

We apply this approach to evaluate $\tilde{\omega}_{\min}^2$ for a grid of equilibrium models spanning $1 \leqslant \beta \leqslant 30$ and $0.00 \leqslant q \leqslant 0.40$. In all cases, we assume an azimuthal wavenumber $m = 1$ and $\gamma = 5/3$. Figure 3 shows a contour map of the resulting values. Plotted over the map are the stability boundaries predicted by the original stability criteria (Equation (53)), the cTI criteria (Equation (54)) and the anTI criteria (Equation (55)). The original criteria over-predict the extent of the instability seen in the numerical calculations, while the cTI criteria under-predict it. Only the anTI criteria correctly predict the stability boundary $\tilde{\omega}_{\min}^2 = 0$, confirming that they are the correct choice for LBR anelastic MHD.

In his dynamo models, Spruit (1999, 2002) assumes that the growth rate of the TI is of the order $\lambda \approx \omega_A$ in the limit where the rotation angular frequency Ω is small compared to the Alfvén frequency ω_A defined by

$$\omega_A^2 = \frac{2m^2 a^2}{\beta r^2}. \tag{58}$$

To compare this assumption against our calculations, we write the ratio of growth rate to Alfvén frequency as

$$\frac{\lambda}{\omega_A} = |\omega| \sqrt{\frac{\beta r^2}{2m^2 a^2}} \lesssim |\tilde{\omega}_{\min}| \sqrt{\frac{\beta(\tilde{r}_a + \tilde{r}_b)^2}{8m^2}}, \tag{59}$$
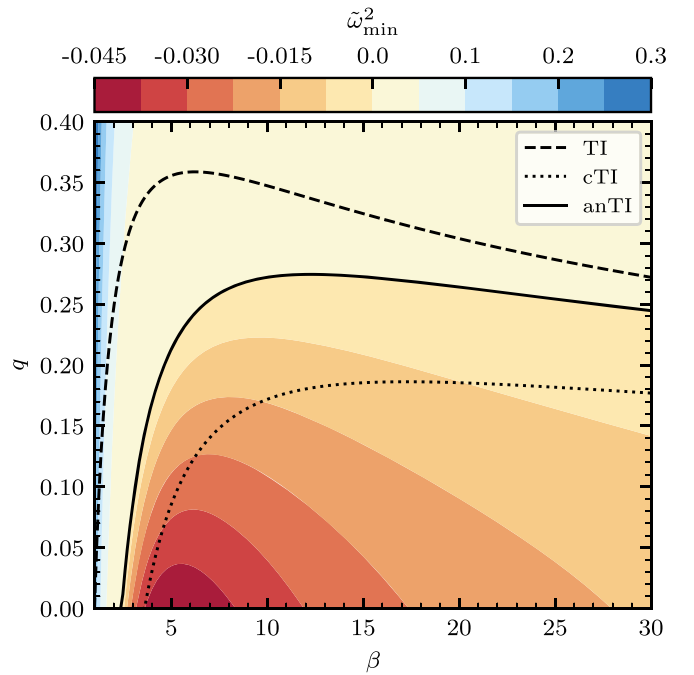

Figure 3. Contour map of the minimal eigenvalue $\tilde{\omega}_{\min}^2$, plotted across the β-q plane for an azimuthal wavenumber $m = 1$ and equilibrium models having $\gamma = 5/3$. Regions where $\tilde{\omega}_{\min}^2 < 0$ are unstable to the Tayler instability. The three black lines show the stability boundaries for the fully compressible criteria (TI), the constrained anelastic criteria (cTI) and the LBR anelastic criteria (anTI). Only the LBR anelastic criteria correctly predict the $\tilde{\omega}_{\min}^2 = 0$ stability boundary.

where the second (in)equality follows from setting $|\tilde{\omega}| = |\tilde{\omega}_{\min}|$, and evaluating the ratio at the midpoint $\tilde{r} = (\tilde{r}_a + \tilde{r}_b)/2$ of the calculation domain. For modes with azimuthal order $m = 1$, we find this ratio has an average value $\lambda/\omega_A \approx 0.27$ over the unstable region plotted in Figure 3, and a maximal value $\lambda/\omega_A \approx 0.42$. These are both moderately smaller than the $\lambda/\omega_A \approx 1$ assumed by Spruit (1999, 2002). Therefore, future studies involving anelastic MHD simulations of the TI should recognize that the growth rate can be smaller than ω_A, and adjust their expectations accordingly.

6. Conclusion

The TI is of interest in the radiative regions of stars because, with differential rotation, it may contribute to forming and maintaining a magnetic field dynamo that could significantly affect the stars' structure and evolution. However, attempts to heuristically derive and numerically simulate the growth and saturation of the TI in stellar models have led to indeterminate results.

The TI criteria were derived using fully compressible MHD, but simulations of fluid dynamics in stellar interiors frequently use some version of the anelastic or pseudo-incompressible approximations, which suppress acoustic waves with much shorter periods than stellar timescales. The goal of this paper was not to address the problem of whether the dynamo exists but to narrow the gap between fully compressible linear theory and anelastic nonlinear simulations of the TI.

We undertook this by modifying the classic MHD energy principle (Bernstein et al. 1958) according to LBR anelastic MHD, which—based on the work of Brown et al. (2012)—we regard as the most promising of several anelastic schemes. We

derived a version of the MHD energy principle that yields stability criteria (Equations (46) and 47) in excellent agreement with solutions of the eigenvalue problem calculated using the GYRE code. Our test configuration was a family of cylindrically symmetric magnetohydrostatic equilibria with a toroidal background magnetic field and gravity supplied by a line mass (Section 5.1). Our results show that the instability still exists in LBR anelastic MHD, but in a more restricted part of parameter space than the fully compressible case. This happens because the energy principle is based on minimizing the potential energy of the system, and anelasticity introduces a constraint which precludes full minimization. However, we conclude that the instability should manifest in anelastic LBR MHD simulations if the models used are unstable under the anTI criteria.

We found that the amplitude of the displacement in the horizontal direction is greater than the displacement in the radial direction, as predicted by Spruit (2002). We also found that the largest growth rates calculated by GYRE are somewhat smaller than predicted for slow rotators by Spruit (2002).

We are limited in addressing discrepancies between our calculations and heuristic predictions of the saturated state because our analysis and numerical calculations are in the linear regime and lack rotation or dissipative effects, both of which are key ingredients in the proposed instability-driven dynamo (Spruit 2002). We are unable to predict the nonlinear growth rate and amplitude of the instabilities without taking those physical effects into consideration. This is beyond the scope of this work, but it is an open question for future work.

Our family of cylindrical models can be implemented in anelastic MHD simulations. These simulations could verify the linear analysis and calculations that we performed, and determine how nonlinear effects impact the growth rate and amplitude of the instability. By choosing models that are unstable under the anTI criteria, and by including differential rotation, anelastic MHD simulations could more accurately test the Tayler–Spruit dynamo and its significance as a mechanism for angular momentum transport in stellar evolution.

Appendix
Numerical Technique

To calculate numerical solutions of the LBR anelastic Equations (19)–(23), (26), we first undertake a separation of variables in space and time, by writing perturbed quantities in the form

$$
\begin{pmatrix} \xi_r \\ \xi_\phi \\ \xi_z \end{pmatrix} = r_0 \operatorname{Re} \left\{ \begin{pmatrix} \tilde{\xi}_r \\ i\tilde{\xi}_\phi \\ i\tilde{\xi}_z \end{pmatrix} \exp[i(m\phi + kz/r_0 + \omega t)] \right\} \quad (60)
$$

$$
\begin{pmatrix} B_r' \\ B_\phi' \\ B_z' \end{pmatrix} = \sqrt{\frac{8\pi P_0}{\beta}} \operatorname{Re} \left\{ \begin{pmatrix} i\tilde{B}_r' \\ \tilde{B}_\phi' \\ \tilde{B}_z' \end{pmatrix} \exp[i(m\phi + kz/r_0 + \omega t)] \right\} \quad (61)
$$

$$
\begin{pmatrix} J_r' \\ J_\phi' \\ J_z' \end{pmatrix} = \frac{c}{4\pi r_0} \sqrt{\frac{8\pi P_0}{\beta}}
$$

$$
\times \operatorname{Re} \left\{ \begin{pmatrix} i\tilde{J}_r' \\ \tilde{J}_\phi' \\ \tilde{J}_z' \end{pmatrix} \exp[i(m\phi + kz/r_0 + \omega t] \right\} \quad (62)
$$

$$
\Pi' = \frac{P_0}{\rho_0} \operatorname{Re} \{\tilde{\Pi}' \exp[i(m\phi + kz/r_0 + \omega t]\} \quad (63)
$$

$$
S' = c_P \operatorname{Re} \{\tilde{S}' \exp[i(m\phi + kz/r_0 + \omega t]\}. \quad (64)
$$

In these expressions, all quantities with a tilde (˜) are dimensionless real functions of r, to be determined numerically; the integer m is the azimuthal wavenumber introduced in Section (4.1); and the real number k is the axial wavenumber. Here, we choose to work with

$$
\Pi' = \varpi' + \frac{B_\phi B_\phi'}{4\pi\rho_0} \quad (65)
$$

rather than the reduced pressure ϖ, as this allows $\tilde{J}_\phi'$ and $\tilde{J}_z'$ to be decoupled from the other dependent variables, reducing the differential order of the system from four to two.

With these definitions, and assuming the equilibrium that we introduce in Section 5.1, we write the linearized equations in the form

$$
\frac{d\boldsymbol{v}}{d\tilde{r}} = \mathbf{A}_{vv}\boldsymbol{v} + \mathbf{A}_{vw}\boldsymbol{w} \quad (66)
$$

$$
\mathbf{0} = \mathbf{A}_{wv}\boldsymbol{v} + \mathbf{A}_{ww}\boldsymbol{w} \quad (67)
$$

where $\tilde{r} \equiv r/r_0$ is the independent variable, and the vectors

$$
\boldsymbol{v} = \begin{pmatrix} \tilde{\xi}_r \\ \tilde{\Pi}' \end{pmatrix}, \qquad \boldsymbol{w} = \begin{pmatrix} \tilde{\xi}_\phi \\ \tilde{\xi}_z \\ \tilde{B}_r' \\ \tilde{B}_\phi' \\ \tilde{B}_z' \\ \tilde{J}_r' \\ \tilde{S}' \end{pmatrix} \quad (68)
$$

contain the dependent variables. The Jacobian matrices in Equations (66) and (67) are given by

$$\mathbf{A}_{vv} = \begin{pmatrix} \frac{\alpha - 1}{\tilde{r}} & 0 \\ \tilde{\omega}^2 & 0 \end{pmatrix}, \tag{69}$$

$$\mathbf{A}_{vw} = \begin{pmatrix} \frac{m}{\tilde{r}} & k & 0 & 0 & 0 & 0 & 0 \\ 0 & 0 & -\frac{2m}{\beta\tilde{r}} & \frac{2(\alpha - 2)}{\beta\tilde{r}} & 0 & 0 & \frac{q}{r} \end{pmatrix}, \tag{70}$$

$$\mathbf{A}_{wv} = \begin{pmatrix} 0 & -\frac{m}{\tilde{r}} \\ 0 & -k \\ \frac{m}{\tilde{r}} & 0 \\ \frac{2 - \alpha}{2\tilde{r}} & 0 \\ 0 & 0 \\ 0 & 0 \\ \frac{\alpha(\gamma - 1)}{\gamma\tilde{r}} & 0 \end{pmatrix}, \tag{71}$$

$$\mathbf{A}_{ww} = \begin{pmatrix} \tilde{\omega}^2 & 0 & \frac{2 - \alpha}{\beta\tilde{r}} & \frac{2m}{\beta\tilde{r}} & 0 & 0 & 0 \\ 0 & \tilde{\omega}^2 & 0 & \frac{2k}{\beta} & 0 & \frac{2}{\beta} & 0 \\ 0 & 0 & -1 & 0 & 0 & 0 & 0 \\ -\frac{m}{\tilde{r}} & 0 & 0 & -1 & 0 & 0 & 0 \\ 0 & -\frac{m}{\tilde{r}} & 0 & 0 & -1 & 0 & 0 \\ 0 & 0 & 0 & -k & \frac{m}{\tilde{r}} & -1 & 0 \\ 0 & 0 & 0 & 0 & 0 & 0 & 1 \end{pmatrix}, \tag{72}$$

where we introduce the dimensionless frequency

$$\tilde{\omega} = \frac{r_0}{a}\omega. \tag{73}$$

By eliminating w between Equations (66) and (67), we arrive at a system of differential equations for v alone:

$$\frac{dv}{d\tilde{r}} = (\mathbf{A}_{vv} - \mathbf{A}_{vw}\mathbf{A}_{ww}^{-1}\mathbf{A}_{wv})v \equiv \mathbf{A}v, \tag{74}$$

where the second equality serves to define the overall Jacobian matrix $\mathbf{A}$. Although we do not write out an explicit expression for the elements of $\mathbf{A}$, we note that each contains a factor

$$F = \frac{1}{\beta\tilde{r}^2\tilde{\omega}^2 - 2m^2} = \frac{1}{\beta\tilde{r}^2(\tilde{\omega}^2 - \tilde{\omega}_A^2)}, \tag{75}$$

where

$$\tilde{\omega}_A = \frac{r_0}{a}\omega_A \tag{76}$$

is the dimensionless equivalent of the Alfvén frequency defined in Equation (58). The factor F diverges if $\tilde{\omega} = \tilde{\omega}_A$, indicating a local resonance with the Alfvén wave. In the present context, such behavior is not a problem because we are interested in finding unstable modes for which $\tilde{\omega}^2 < 0$, and therefore the resonance never arises.

Together with the boundary conditions

$$v_1 = \tilde{\xi}_r = 0 \tag{77}$$

on the inner ($\tilde{r} = \tilde{r}_a$) and outer ($\tilde{r} = \tilde{r}_b$) boundaries of the calculation domain (in accordance with Equation (32)), the system of Equations (74) is a linear two-point boundary eigenvalue problem (BVEP), with $\tilde{\omega}^2$ serving as the eigenvalue. To solve the BVEP numerically we use the GYRE code (Townsend & Teitler 2013). Although GYRE is designed to address stellar pulsation problems, it is built on a robust multiple-shooting scheme that can in principle be applied to any BVEP. Accordingly, we modify GYRE to implement the differential equations and boundary conditions given here. The modified code takes as inputs parameters specifying the equilibrium model (β, γ, q), the wavenumbers (m, k), and the calculation domain ($\tilde{r}_a$, $\tilde{r}_b$, and the number of points N used to discretize the differential equations). As outputs, it calculates the eigenvalues $\tilde{\omega}^2$ of the discrete modal solutions, and the corresponding eigenfunctions given by the components of v and w.

ORCID iDs

E. G. Zweibel ⓘ https://orcid.org/0000-0003-4821-713X

References

Acheson, D. J. 1978, RSPTA, 289, 459
Aurière, M., Wade, G. A., Silvester, J., et al. 2007, A&A, 475, 1053
Bernstein, I. B., Frieman, E. A., Kruskal, M. D., & Kulsrud, R. M. 1958, RSPSA, 244, 17
Braginsky, S. I., & Roberts, P. H. 1995, GApFD, 79, 1
Braithwaite, J. 2006a, A&A, 453, 687
Braithwaite, J. 2006b, A&A, 449, 451
Brown, B. P., Vasil, G. M., & Zweibel, E. G. 2012, ApJ, 756, 109
Cantiello, M., Mankovich, C., Bildsten, L., Christensen-Dalsgaard, J., & Paxton, B. 2014, ApJ, 788, 93
Denissenkov, P. A., & Pinsonneault, M. 2007, ApJ, 655, 1157
Fuller, J., Piro, A. L., & Jermyn, A. S. 2019, MNRAS, 485, 3661
Heger, A., Woosley, S. E., & Spruit, H. C. 2005, ApJ, 626, 350
Kulsrud, R. 1964, Proc. of the International School of Physics "Enrico Fermi," Advances Plasma Theory, ed. M. N. Rosenbluth, (New York: Academic Press), 54
Lantz, S. R. 1992, PhD thesis, Cornell Univ.
Maeder, A., & Meynet, G. 2003, A&A, 411, 543
Maeder, A., & Meynet, G. 2004, A&A, 422, 225
Maeder, A., & Meynet, G. 2005, A&A, 440, 1041
Markey, P., & Tayler, R. J. 1973, MNRAS, 163, 77
Markey, P., & Tayler, R. J. 1974, MNRAS, 168, 505
Meynet, G., & Maeder, A. 2005, A&A, 429, 581
Paxton, B., Cantiello, M., Arras, P., et al. 2013, ApJS, 208, 4
Paxton, B., Marchant, P., Schwab, J., et al. 2015, ApJS, 220, 15
Paxton, B., Schwab, J., Bauer, E. B., et al. 2018, ApJS, 234, 34
Pitts, E., & Tayler, R. J. 1985, MNRAS, 216, 139
Song, H. F., Meynet, G., Maeder, A., et al. 2018, A&A, 609, A3
Song, H. F., Meynet, G., Maeder, A., Ekström, S., & Eggenberger, P. 2016, A&A, 585, A120
Spruit, H. C. 1999, A&A, 349, 189
Spruit, H. C. 2002, A&A, 381, 923
Tayler, R. J. 1973, MNRAS, 161, 365
Townsend, R. H. D., & Teitler, S. A. 2013, MNRAS, 435, 3406
Zahn, J.-P., Brun, A. S., & Mathis, S. 2007, A&A, 474, 145